PHYSICAL REVIEW B **76**, 205307 (2007)

Enhanced spin-orbit scattering length in narrow $Al_xGa_{1-x}N/GaN$ wires

Patrick Lehnen, Thomas Schäpers,* Nicoleta Kaluza, Nicolas Thillosen, and Hilde Hardtdegen
Institute of Bio- and Nanosystems (IBN-1), cni-Center of Nanoelectronic Systems for Information Technology, and Virtual Institute of Spinelectronics (VISel), Research Centre Jülich GmbH, 52425 Jülich, Germany
(Received 24 April 2007; revised manuscript received 28 July 2007; published 6 November 2007)

The magnetotransport in a set of identical parallel $Al_xGa_{1-x}N/GaN$ quantum wire structures is investigated. The width of the wires ranges between 1110 and 340 nm. For all sets of wires, clear Shubnikov–de Haas oscillations are observed. We find that the electron concentration and mobility are approximately the same for all wires, confirming that the electron gas in the $Al_xGa_{1-x}N/GaN$ heterostructure is not deteriorated by the fabrication procedure of the wire structures. For the wider quantum wires, the weak antilocalization effect is clearly observed, indicating the presence of spin-orbit coupling. For narrow quantum wires with an effective electrical width below 250 nm, the weak antilocalization effect is suppressed. By comparing the experimental data to a theoretical model for quasi-one-dimensional structures, we come to the conclusion that the spin-orbit scattering length is enhanced in narrow wires.

DOI: 10.1103/PhysRevB.76.205307 PACS number(s): 73.20.Fz, 73.43.Qt, 72.25.Rb, 73.61.Ey

I. INTRODUCTION

The $Al_xGa_{1-x}N/GaN$ material system is a very promising candidate for future spin electronic applications. The reason is that two important requirements for the realization of spin electronic devices are fulfilled in this material class. First, transition-metal-doped GaN diluted magnetic semiconductors have been shown to have high Curie temperatures for injection and detection of spin polarized carriers (see, e.g., Ref. 1 and references therein). Second, spin-orbit coupling for spin control in nonmagnetic $Al_xGa_{1-x}N/GaN$ heterostructures was observed.[2–11]

Spin-orbit coupling in $Al_xGa_{1-x}N/GaN$ two-dimensional electron gases (2DEGs) can be investigated by analyzing the characteristic beating pattern in Shubnikov–de Haas oscillations,[2–5] by measuring the circular photogalvanic effect,[6] or by studying weak antilocalization.[4,7,9–11] The latter is an electron interference effect where the random deviations of the spin orientations between time-reversed paths result in an enhanced conductance.[12–14] From weak antilocalization measurements, information on characteristic length scales, i.e., the spin-orbit scattering length l_{so} and the phase coherence length l_ϕ, can be obtained.

For quasi-one-dimensional systems, it was predicted theoretically[15–18] and shown experimentally[19–22] that l_{so} can be considerably enhanced compared to the value of the 2DEG. This has important implications for the performance of spin electronic devices, e.g., the spin field-effect transistor,[23] since an enhanced value of l_{so} results in a larger degree of spin polarization in the channel and thus in larger signal modulation.[15,23] In addition, many of the recently proposed novel spin electronic device structures explicitly make use of one-dimensional channels because the restriction to only one dimension allows new switching schemes.[24–27]

Very recently, transport measurements on AlGaN/GaN -based one-dimensional structures, i.e., quantum point contacts, have been reported.[8,28] With respect to possible spin electronic applications, it is of great interest how the spin transport takes place in AlGaN/GaN quasi-one-dimensional structures. Since an enhanced value of l_{so} is very advantageous for the design of spin electronic devices, it would be very desirable if this effect can be observed in $Al_xGa_{1-x}N/GaN$ wire structures.

Here, we report on magnetotransport measurements on $Al_xGa_{1-x}N/GaN$ parallel quantum wire structures. We will begin by discussing the basic transport properties of wires with different widths, i.e., resistivity, sheet electron concentration, and mobility. Spin-orbit coupling in our $Al_xGa_{1-x}N/GaN$ quantum wires is investigated by analyzing the weak antilocalization effect. We will discuss to which extent the weak antilocalization effect in $Al_xGa_{1-x}N/GaN$ heterostructures is affected by the additional confinement in wire structures. By fitting a theoretical model to our experimental data, we will be able to answer the question if the spin-orbit scattering length increases with decreasing wire width, as found in quantum wires fabricated from other types of heterostructures.

II. EXPERIMENT

The AlGaN/GaN heterostructures were grown by metal organic vapor phase epitaxy on a (0001) Al_2O_3 substrate. Two different samples were investigated. Sample 1 consisted of a 3-μm-thick GaN layer followed by a 35-nm-thick $Al_{0.20}Ga_{0.80}N$ top layer, while in sample 2 a 40-nm-thick $Al_{0.10}Ga_{0.90}N$ layer was used as a top layer. The quantum wire structures were prepared by first defining a Ti etching mask using electron beam lithography and lift-off. Subsequently, the AlGaN/GaN wires were formed by Ar^+ ion beam etching. The etching depth of 95 nm was well below the depth of the AlGaN/GaN interface. The electron beam lithography pattern was chosen so that a number of 160 identical wires, each 620 μm long, were connected in parallel. A schematic cross section of the parallel wires is shown in Fig. 1 (inset).

Different sets of wires were prepared, comprising a geometrical width W ranging from 1110 down to 340 nm (see Table I). The geometrical widths of the wires were determined by means of scanning electron microscopy. The sample geometry with quantum wires connected in parallel

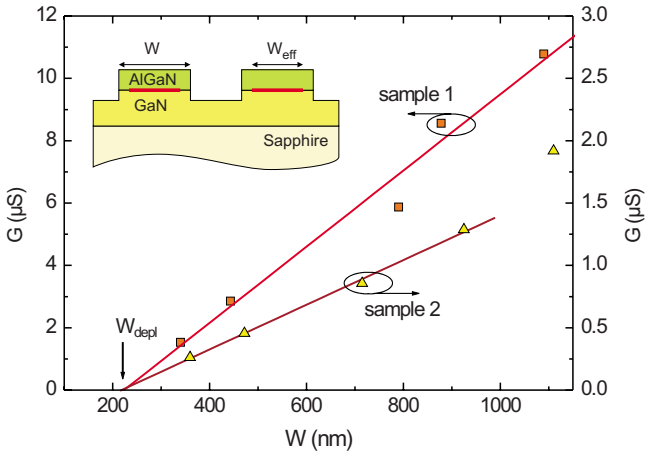

FIG. 1. (Color online) Conductance G as a function of the geometrical width W. The conductance of a single wire is plotted, which was determined by dividing the total conductance by the number of wires connected in parallel. The full lines represent the corresponding linear fits. The arrows indicate the total width of the depletion zones W_{depl}. The inset shows a schematics of the cross section of the wires. Here, W corresponds to the geometrical width, while W_{eff} indicates the effective electrical width.

was chosen in order to suppress universal conductance fluctuations.[29] After removing the Ti mask by HF, Ti/Al/Ni/Au Ohmic contacts were defined by optical lithography. The Ohmic contacts were alloyed at 900 °C for 30 s. For reference purposes, a 100-μm-wide Hall bar structure with voltage probes separated by a distance of 410 μm was prepared on the same chip.

The measurements were performed in a He^3 cryostat at temperatures ranging from 0.4 to 4.0 K. The resistances were measured by employing a current-driven lock-in technique with an ac excitation current of 100 nA and 1 μA for samples 1 and 2, respectively.

III. RESULTS AND DISCUSSION

In order to gain information on the transport properties of the $Al_xGa_{1-x}N/GaN$ layer systems, Shubnikov–de Haas oscillations were measured on the Hall bar samples. At a temperature of 0.5 K, sheet electron concentrations n_{2D} of 5.1×10^{12} and 2.2×10^{12} cm^{-2} were determined for samples 1 and 2, respectively. The Fermi energies calculated from n_{2D} are 55 meV for sample 1 and 24 meV for sample 2. Here, an effective electron mass of $m^*=0.22m_e$ was taken into account.[9] The mobilities μ were 9150 and 3930 cm^2/V s for samples 1 and 2, respectively, resulting in elastic mean free paths l_{el} of 314 and 95 nm. The smaller electron concentration of sample 2 can be attributed to the lower Al content of the $Al_xGa_{1-x}N$ barrier layer, resulting in smaller polarization doping.[31] The lower mobility found in sample 2 compared to sample 1 can be explained by the reduced screening at lower electron concentrations.[32]

Owing to the large surface potential of GaN, which has been determined to be between 0.5 and 0.6 eV,[33] a considerable surface carrier depletion can be expected. For our wires, the carrier depletion at the mesa edges will result in an effective electrical width W_{eff}, which is smaller than the measured geometrical width W. In order to gain information on the lateral width of the depletion zone, the wire conductance at zero magnetic field was determined for different wire widths. In Fig. 1, the single-wire conductance G is shown as a function of the wire width for both samples. It can be seen that for both samples, G scales linearly with W. The total width of the depletion zone was determined from the linear extrapolation to $G=0$, indicated by W_{depl} in Fig. 1.[34,35] The depletion zone width for sample 1 is 210 nm, while for sample 2 a value of 240 nm was determined. The larger value of W_{depl} for sample 2 can be attributed to the lower electron concentration compared to sample 1. The corresponding effective electrical width W_{eff}, defined by $W - W_{depl}$, is listed in Table I. The two-dimensional resistivity ρ of the wires at $B=0$ was calculated based on W_{eff}. As can be

TABLE I. Summary of characteristic parameters of both samples: The sample number, geometrical wire width W, effective electrical wire width W_{eff}, resistivity ρ, sheet electron concentration n_{2D}, mobility μ, and elastic mean free path l_{el}. The spin-orbit scattering length l_{so}, and phase coherence length l_ϕ were extracted from the fit using the Kettemann model.[30]

#	W (nm)	W_{eff} (nm)	ρ (Ω)	n_{2D} (10^{12} cm^{-2})	μ (cm^2/V s)	l_{el} (nm)	l_{so} (nm)	l_ϕ (nm)
1	1090	880	131	5.1	9400	349	550	3000
1	880	670	126	5.2	9600	360	600	2950
1	690	480	132	4.9	9700	344	700	2500
1	440	230	132	5.2	9000	341	1300	1550
1	340	130	136	4.5	10000	343	>1800	1150
2	1110	870	730	2.2	4000	96	500	1200
2	930	690	860	2.2	3400	82	520	1000
2	720	480	900	2.0	3400	81	640	950
2	470	230	830	2.0	3800	88	>850	900
2	360	120	740	1.9	4300	100	>1000	670

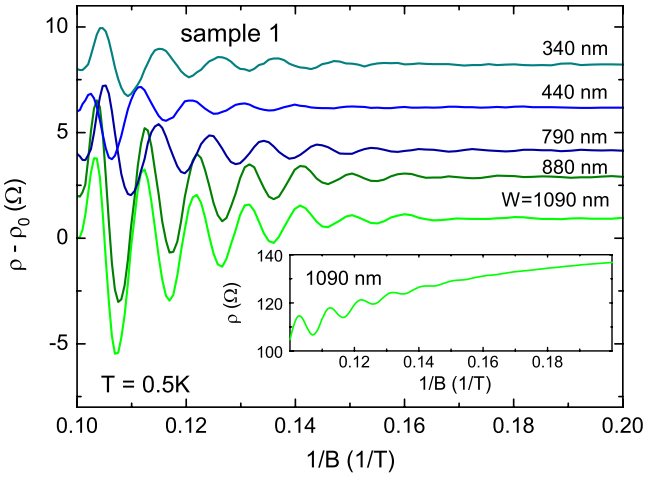

FIG. 2. (Color online) Magnetoresistivity as a function of the inverse magnetic field for a set of wires of different widths (sample 1). The slowly varying background resistivity $\rho_0(B)$ was subtracted. For clarity, the curves are offset by 2 Ω. The resistance of the sets of wires was measured at a temperature of 0.5 K. The inset shows the resistivity of the 1090-nm-wide wires before the background resistivity $\rho_0(B)$ was subtracted.

seen by the values of ρ given in Table I, for sample 1 the resistivity remains at approximately the same value if the wire width is reduced. A similar behavior is observed for sample 2, although the variations are somewhat larger. In any case, no systematic change of ρ is found for both samples.

As can be seen in Fig. 2, clear Shubnikov–de Haas oscillations in the magnetoresistivity $\rho(B)-\rho_0(B)$ are resolved for different sets of wires of sample 1. For a better comparison, the slowly varying field-dependent background resistivity $\rho_0(B)$ was subtracted. In order to get an impression on the relation between the amplitude of the Shubnikov–de Haas oscillations and the background resistivity, the total resistivity $\rho(B)$ is shown exemplarily for the 1090-nm-wide wires in Fig. 2 (inset). As can be seen here, the oscillation amplitude turns out to be small compared to $\rho_0(B)$ because of the relatively low mobility. From the oscillation period of $\rho(B)-\rho_0(B)$ vs $1/B$, the sheet electron concentration n_{2D} was determined for the different sets of wires. As can be seen in Fig. 2, the oscillation period, and thus n_{2D}, is approximately the same for all sets of wires (Table I). The values of n_{2D} are comparable to the value found for the 2DEG. As given in Table I, for sample 2 the values of n_{2D} for the different sets of wires were also found to be close to the value extracted from the corresponding Hall bar structure.

The mobility μ and elastic mean free path l_{el} was determined from n_{2D} and $\rho(B=0)$. As can be inferred from the values of μ and l_{el} given in Table I, both quantities are similar for all sets of wires for a given heterostructure. For sample 2, l_{el} is always smaller than W_{eff}; therefore, no significant deviation from the 2DEG conductivity is expected. However, for the 440- and 340-nm-wide wires of sample 1, l_{el} exceeds W_{eff} so that a boundary scattering contribution is expected. However, since the mobility is not decreased, we can conclude that the boundary scattering is predominately specular. Probably, the smooth potential from the depletion zone favors specular reflection.

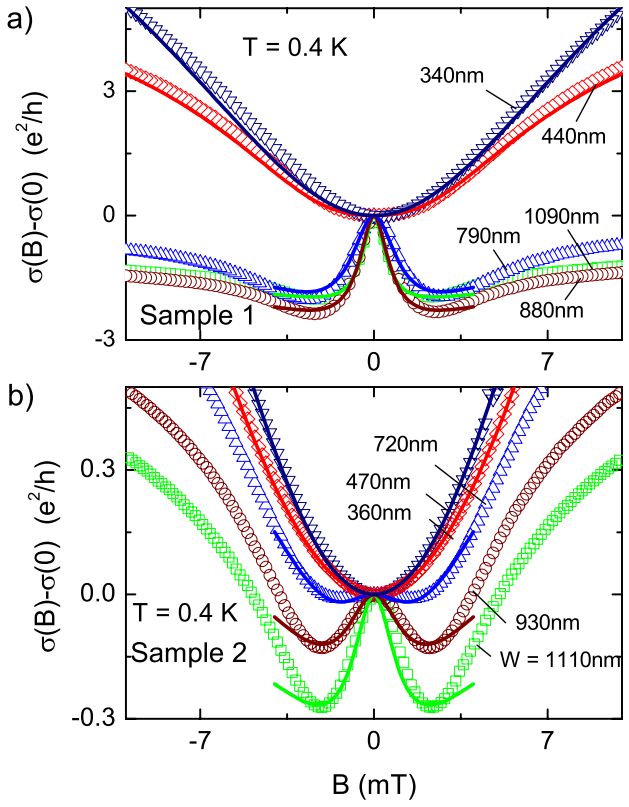

FIG. 3. (Color online) (a) Experimental magnetoconductivity $\sigma(B)-\sigma(0)$ normalized to e^2/h for different sets of wires of sample 1. The measurement temperature was 0.4 K. Sets of wires with a geometrical width ranging from 1090 down to 340 nm were measured. The full lines show the calculated values using the Kettemann model (Ref. 30). (b) Corresponding measurements of $\sigma(B)-\sigma(0)$ for sets of wires of sample 2 with widths in the range from 1110 to 360 nm. The full lines show the calculated magnetoconductivity.

We now turn to the investigation of spin-related effects in the electron transport. In Fig. 3(a), the normalized magnetoconductivity $\sigma(B)-\sigma(0)$ is shown for different sets of wires of sample 1. For the narrow wires with a width up to 440 nm, the magnetoconductivity monotonously increases for increasing values of $|B|$, which can be attributed to weak localization. The weak localization effect originates from the constructive interference of time-reversed paths for the case when spin-orbit scattering can be neglected. In contrast, for the 1090-, 880-, and 790-nm-wide wires, a peak is found in the magnetoconductivity at $B=0$, which is due to weak antilocalization. The slope of the magnetoconductivity changes sign at $|B| \approx 2.2$ mT. This value corresponds well to the positions of the minima found in the weak antilocalization measurements on the Hall bars of sample 1. For magnetic fields beyond 2.2 mT, the transport is governed by weak localization, where the magnetoconductivity increases with $|B|$.

As can be seen in Fig. 3(b), a similar behavior is found for sample 2. For wire widths up to 470 nm, weak localization is observed, whereas for the 1110-, 930-, and 720-nm-wide wires, weak antilocalization is found. In contrast to sample 1, the width of the weak antilocalization peak depends on the

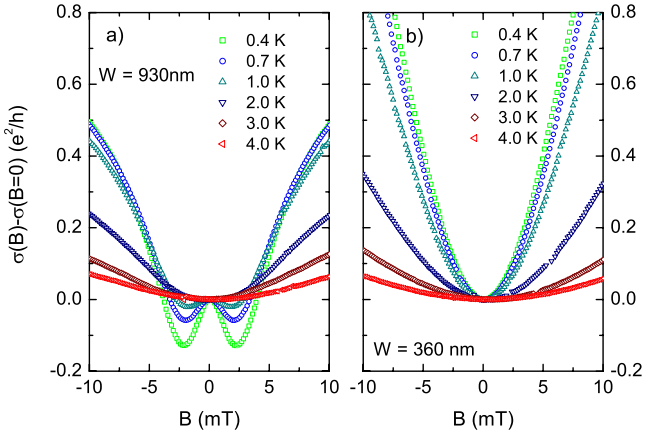

FIG. 4. (Color online) (a) Magnetoconductivity $\sigma(B)-\sigma(0)$ normalized to e^2/h of the 930-nm-wide set of wires of sample 2 at different temperatures in the range from 0.4 to 4 K. (b) Corresponding measurements for the set of 360-nm-wide wires.

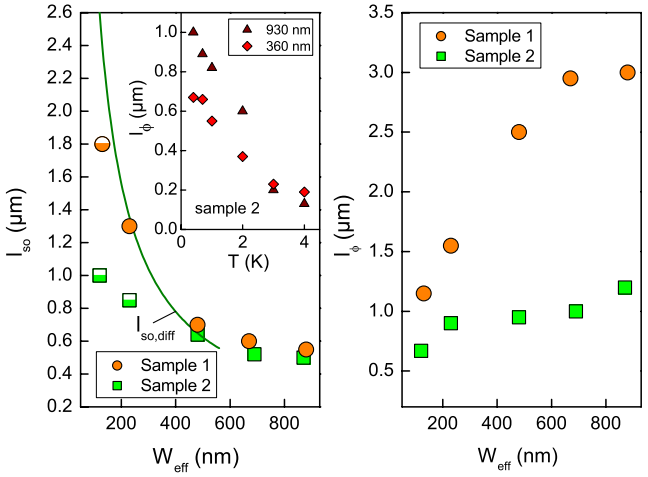

FIG. 5. (Color online) (a) Spin-orbit scattering length l_{so} determined from the fit of the Kettemann model (Ref. 30) to the $\sigma(B)-\sigma(0)$ curves at $T=0.4$ K for sample 1 (circles) and sample 2 (squares). The half filled symbols at small width represent the lower boundary values of l_{so}. The inset shows l_ϕ as a function of temperature for the 930- and 360-nm-wide wires of sample 2. (b) Phase coherence length l_ϕ for both samples determined from the fit.

widths of the wires. For the first two sets of wires, minima in $\sigma(B)-\sigma(0)$ are found at $B=\pm 2.2$ mT, whereas for the 720-nm-wide wires, minima are observed at ±1.5 mT. The peak height due to weak antilocalization decreases with decreasing wire width. In general, the modulations of $\sigma(B)-\sigma(0)$ are found to be considerably smaller for sample 2 compared to sample 1, which can be attributed to the smaller elastic mean free path and, as it will be shown later, to the smaller phase coherence length.

With increasing temperature, the weak antilocalization peak decreases. This can be seen in Fig. 4(a), where $\sigma(B)-\sigma(0)$ is shown at different temperatures for the 930-nm-wide wires of sample 2. Above 2 K, no signature of weak antilocalization is found anymore. Furthermore, the weak localization contribution to $\sigma(B)-\sigma(0)$ successively decreases with increasing temperature. This effect can be attributed to the decreasing phase coherence length with increasing temperature.[36,37] As can be seen in Fig. 4(b), for the 360-nm-wide wires, only weak localization was observed. Similar to the wider sets of wires, the weak localization effect is damped with increasing temperatures.

From weak antilocalization measurements, the characteristic length scales, i.e., l_ϕ and l_{so}, can be estimated. In order to get some reference value for the 2DEG, the model developed by Iordanskii, Lyanda-Geller and Pikus[38] (ILP model) was fitted to the weak antilocalization measurements of the Hall bar structures. Only the Rashba contribution was considered, here. For sample 1, l_ϕ and l_{so} were found to be 1980 and 300 nm at 0.5 K, respectively, whereas for sample 2, the corresponding values were 1220 and 295 nm at 0.4 K. For both samples, the effective spin-orbit coupling parameter $\alpha=\hbar^2/2m^* l_{so}$ is approximately 5.8×10^{-13} eV m. The zero-field spin-splitting energy can be estimated by using the expression $\Delta_{so}=2k_F\alpha$, with the Fermi wave number k_F given by $\sqrt{2\pi n_{2D}}$. For sample 1 one obtains a value of $\Delta_{so}=0.66$ meV, while for sample 2 one finds 0.43 meV. The values of Δ_{so} are relatively large compared to their corresponding Fermi energies, which confirms the presence of a pronounced spin-orbit coupling in $Al_xGa_{1-x}N/GaN$ 2DEGs.[7,9–11]

The ILP model is only valid for 2DEGs with $l_\phi \ll W$; thus, it cannot be applied to our wire structures. Very recently, a model appropriate for wire structures was developed by Kettemann,[30] which covers the case $W<l_\phi$. Here, the quantum correction to the conductivity is given by

$$\sigma(B)-\sigma(0)=\frac{e^2}{h}\left(\frac{\sqrt{H_W}}{\sqrt{H_\phi+B^*/4}}-\frac{\sqrt{H_W}}{\sqrt{H_\phi+B^*/4+H_{so}}}-2\frac{\sqrt{H_W}}{\sqrt{H_\phi+B^*/4+H_{so}/2}}\right), \quad (1)$$

with H_ϕ defined by $\hbar/(4el_\phi^2)$ and H_W given by $\hbar/(4eW_{eff}^2)$. The effective external magnetic field B^* is defined by

$$B^*=B\left(1-\frac{1}{1+W_{eff}^2/3l_B^2}\right), \quad (2)$$

with $l_B=\sqrt{\hbar/eB}$ as the magnetic length. The spin-orbit scattering length l_{so} in the wire can be obtained from the characteristic spin-orbit field $H_{so}=\hbar/(4el_{so}^2)$.

The Kettemann model was fitted to the experimental curves by adjusting H_{so} and H_ϕ. The corresponding values of l_{so} and l_ϕ extracted from the fit are listed in Table I and shown in Fig. 5. Even for the widest wires, l_{so} is found to be larger than the value obtained for the 2DEG from the ILP fit. The deviations are probably already due to confinement effects. In addition, different approximations made in the ILP model[38] for the two-dimensional case and the Kettemann model[30] for wire structures might also account partially for the deviations.

As can been seen in Fig. 5, for sample 1, the spin-orbit scattering length l_{so} monotonously increases with decreasing W_{eff}, while l_ϕ decreases. The latter is in accordance to theoretical predictions.[36,37] For the wider wires with $W=1090$,

880, and 790 nm, l_ϕ exceeds l_{so}, so that weak antilocalization is expected. In contrast, for the very narrow wires with W_{eff}=230 and 130 nm, the values for l_{so} obtained from the fit are close to or even exceed l_ϕ. In this case, the spin rotation caused by spin-orbit coupling is not sufficiently strong to affect the interference of time-reversed paths.[39] As a consequence, the weak antilocalization effect is suppressed so that weak localization remains. For the 340-nm-wide wires, a satisfactory fit could be obtained down to a lower boundary value of l_{so}, indicated by the half filled symbol shown in Fig. 5(a). In principle, one could argue that the appearance of weak localization for the very narrow wires is solely due to a strongly reduced phase coherence length, while l_{so} remains at the relatively low values found for the wider wires. However, in our fits, the suppression of the weak antilocalization effect could not be explained by simply decreasing l_ϕ compared to the values of the wider wires. A satisfactory fit was only obtained if l_{so} was increased to a larger value compared to the wider wires.

As can be seen in Fig. 5, for sample 2, the spin-orbit scattering length l_{so} also increases with decreasing W_{eff}, although with a smaller slope, compared to sample 1. Similarly to sample 1, l_ϕ decreases with decreasing wire width. However, due to the lower elastic mean free path of sample 2, l_ϕ is considerably smaller for this sample (Fig. 5). All values of l_{so} and l_ϕ obtained from the fit are listed in Table I. A comparison of $\sigma(B)-\sigma(0)$ for the widest wires and for the Hall bar structures reveals that the weak antilocalization peak is larger by a factor of 2. Thus, although l_{el} is significantly smaller than W_{eff}, this clearly indicates that the additional carrier confinement already affects the interference effects.[29]

By fitting the Kettemann model to the measurements shown in Fig. 4, l_ϕ was determined for the 930- and 360-nm-wide wires at different temperatures. For both samples, a fixed value of l_{so}, corresponding to the values at 0.4 K, were assumed. As can be seen in Fig. 5(a), inset, for both samples l_ϕ monotonously decreases with temperature, in accordance with theoretical models.[36,37] At a temperature of 4 K, l_ϕ is found to be close to l_{el}. In that regime, the interference effects are expected to be suppressed. This is confirmed by the measurements where only a weak field dependence of $\sigma(B)-\sigma(0)$ is found.

For both samples, we found an increase of l_{so} with decreasing wire width and even a suppression of weak antilocalization for narrow wires. This observance is in accordance with weak antilocalization measurements of quantum wires based on low-band-gap materials, i.e., InGaAs or InAs.[19,20] However, for these types of quantum wells, the coupling parameter α is usually very large. In this case, transport takes place in a different regime where $l_{so} \ll l_{el}$ so that a more elaborate model had to be applied to extract l_{so}.[19] As discussed by Kettemann,[30] the increase of l_{so} can be attributed solely to a modification of the backscattering amplitude. In an intuitive picture, the increase of l_{so} in narrow wires can be explained, by the reduced magnitude of accumulated random spin phases due to the elongated shape of relevant closed loops. Here, the spin phase accumulated in the forward direction is basically compensated by the propagation in the backward direction, so that the spin-related contribution to the interference of electrons backscattered on time-reversed paths tends to diminish. As a result, only weak localization is observed.[15,19] Although the spin-orbit coupling strength in our AlGaN/GaN samples is small compared to heterostructures based on InAs and, thus, different models have to be consulted for a detailed description, the basic mechanism responsible for a suppression of the weak antilocalization effect is the same for both material systems. In our case, no decrease of spin-orbit coupling strength, quantified by α, is required to account for the suppression of weak antilocalization in narrow wires. In fact, an estimation of the effect of the confinement potential on α based on the theory of Moroz and Barnes[40] confirmed that for our wire structures no significant change of α with W_{eff} is expected. As shown in Fig. 5(a), for sample 2 the increase of l_{so} with decreasing wire width is smaller than for sample 1. We attribute this to the fact that for sample 2 the larger extent of diffusive motion, quantified by the smaller value of l_{el}, partially masks the effect of carrier confinement. Due to the larger values of l_{el} and l_ϕ of sample 1 compared to sample 2, the shape of the loops responsible for the interference effect is affected more by the confinement of the wire. Thus, the enhancement of l_{so} is expected to be stronger. Indeed, theoretical calculations by Pareek and Bruno[18] showed that for quasi-one-dimensional channels a strong increase of l_{so} can only be expected if W_{eff} is in the order of l_{el}.

For narrow wires with $W_{eff} < l_{so}$ in the diffusive regime ($l_{el} < W_{eff}$), the spin-orbit scattering lengths can be estimated by[30]

$$l_{so,diff} = \sqrt{12}\frac{l_{so,2D}}{W_{eff}} l_{so,2D}. \tag{3}$$

Here, $l_{so,2D}$ is the spin-orbit scattering length of the 2DEG. The calculated values of $l_{so,diff}$ should only be compared to the fitted values of l_{so} of sample 2 since only for this sample is $l_{el} < W_{eff}$ fulfilled. As can be seen in Fig. 5(a), l_{so} calculated from Eq. (3) fits well to the experimental values corresponding to an intermediate effective wire width of W_{eff} =480 nm. However, for smaller effective wire widths, the calculated values of $l_{so,diff}$ are considerably larger. Probably, spin scattering processes other than the pure Rashba contribution are responsible for this discrepancy.[30]

An enhanced spin-orbit scattering length is very desirable for spin electronic devices. Providing that the strength of the spin-orbit coupling itself remains unchanged, a confinement to a quasi-one-dimensional system would result in a reduced spin randomization. A reduction of spin randomization is an advantage for the realization of spin electronic devices since it would ease the constraints regarding the size of these type of devices. In this respect, our finding that l_{so} increases with decreasing wire width is an important step toward the realization of spin electronic devices based on AlGaN/GaN heterostructures.

IV. CONCLUSIONS

In conclusion, the magnetotransport of AlGaN/GaN quantum wires had been investigated. Even for sets of quantum wires with a geometrical width as low as 340 nm, clear Shubnikov–de Haas oscillations were observed. Magne-

totransport measurements close to zero magnetic field revealed a suppression of the weak antilocalization effect for very narrow quantum wires. By comparing the experimental data with a theoretical model for one-dimensional structures, it was found that the spin-orbit scattering length is enhanced in narrow wires. The observed phenomena might have an important implication regarding the realization of spin electronic devices based on AlGaN/GaN heterostructures.

ACKNOWLEDGMENTS

The authors are very thankful to S. Kettemann, Hamburg University, for fruitful discussions and to H. Kertz for assistance during low temperature measurements.

*th.schaepers@fz-juelich.de

[1] C. Liu, F. Yun, and H. Morkoç, J. Mater. Sci.: Mater. Electron. **16**, 555 (2005).
[2] I. Lo *et al.*, Phys. Rev. B **65**, 161306(R) (2002).
[3] K. Tsubaki, N. Maeda, T. Saitoh, and N. Kobayashi, Appl. Phys. Lett. **80**, 3126 (2002).
[4] J. Lu *et al.*, Appl. Phys. Lett. **85**, 3125 (2004).
[5] K. Cho, T.-Y. Huang, H.-S. Wang, M.-G. Lin, T.-M. Chen, C.-T. Liang, and Y. F. Chen, Appl. Phys. Lett. **86**, 222102 (2005).
[6] W. Weber, S. Ganichev, Z. Kvon, V. Bel'kov, L. Golub, S. Danilov, D. Weiss, W. Prettl, H.-I. Cho, and J.-H. Lee, Appl. Phys. Lett. **87**, 262106 (2005).
[7] N. Thillosen, Th. Schäpers, N. Kaluza, H. Hardtdegen, and V. A. Guzenko, Appl. Phys. Lett. **88**, 022111 (2006).
[8] S. Schmult, M. J. Manfra, A. M. Sergent, A. Punnoose, H. T. Chou, D. Goldhaber-Gordon, and R. J. Molnar, Phys. Status Solidi B **243**, 033302 (2006).
[9] N. Thillosen, S. Cabañas, N. Kaluza, V. A. Guzenko, H. Hardtdegen, and Th. Schäpers, Phys. Rev. B **73**, 241311(R) (2006).
[10] S. Schmult, M. J. Manfra, A. Punnoose, A. M. Sergent, K. W. Baldwin, and R. J. Molnar, Phys. Rev. B **74**, 033302 (2006).
[11] Ç. Kurdak, N. Biyikli, Ü. Özgür, H. Morkoç, and V. I. Litvinov, Phys. Rev. B **74**, 113308 (2006).
[12] S. Hikami, A. I. Larkin, and Y. Nagaoka, Prog. Theor. Phys. **63**, 707 (1980).
[13] G. Bergmann, Solid State Commun. **42**, 815 (1982).
[14] G. M. Gusev, Z. D. Kvon, and V. N. Ovsyuk, J. Phys. C **17**, L683 (1984).
[15] A. Bournel, P. Dollfus, P. Bruno, and P. Hesto, Eur. Phys. J.: Appl. Phys. **4**, 1 (1998).
[16] A. G. Mal'shukov and K. A. Chao, Phys. Rev. B **61**, R2413 (2000).
[17] A. A. Kiselev and K. W. Kim, Phys. Rev. B **61**, 13115 (2000).
[18] T. P. Pareek and P. Bruno, Phys. Rev. B **65**, 241305(R) (2002).
[19] Th. Schäpers, V. A. Guzenko, M. G. Pala, U. Zülicke, M. Governale, J. Knobbe, and H. Hardtdegen, Phys. Rev. B **74**, 081301(R) (2006).
[20] A. Wirthmann, Y. S. Gui, C. Zehnder, D. Heitmann, C.-M. Hu, and S. Kettemann, Physica E (Amsterdam) **34**, 493 (2006).
[21] A. W. Holleitner, V. Sih, R. C. Myers, A. C. Gossard, and D. D. Awschalom, Phys. Rev. Lett. **97**, 036805 (2006).
[22] J. H. Kwon, H. C. Koo, J. Chang, S.-H. Han, and J. Eom, Appl. Phys. Lett. **90**, 112505 (2007).
[23] S. Datta and B. Das, Appl. Phys. Lett. **56**, 665 (1990).
[24] J. Nitta, F. E. Meijer, and H. Takayanagi, Appl. Phys. Lett. **75**, 695 (1999).
[25] A. A. Kiselev and K. W. Kim, Appl. Phys. Lett. **78**, 775 (2001).
[26] M. Governale, D. Boese, U. Zülicke, and C. Schroll, Phys. Rev. B **65**, 140403(R) (2002).
[27] A. W. Cummings, R. Akis, and D. K. Ferry, Appl. Phys. Lett. **89**, 172115 (2006).
[28] H. T. Chou, S. Lüscher, D. Goldhaber-Gordon, M. J. Manfra, A. M. Sergent, K. W. West, and R. J. Molnar, Appl. Phys. Lett. **86**, 073108 (2005).
[29] C. W. J. Beenakker and H. van Houten, Rev. Mod. Phys. **69**, 731 (1997).
[30] S. Kettemann, Phys. Rev. Lett. **98**, 176808 (2007).
[31] O. Ambacher, B. Foutz, J. Smart, J. R. Shealy, N. G. Weimann, K. Chu, M. Murphy, A. J. Sierakowski, W. J. Schaff, and L. F. Eastman, J. Appl. Phys. **87**, 334 (2000).
[32] M. Sakowicz, R. Tauk, J. Lusakowski, A. Tiberj, W. Knap, Z. Bougrioua, M. Azize, P. Lorenzini, K. Karpierz, and M. Grynberg, J. Appl. Phys. **100**, 113726 (2006).
[33] M. Kocan, A. Rizzi, H. Lüth, S. Keller, and U. K. Mishra, Phys. Status Solidi B **234**, 773 (2002).
[34] A. Menschig, A. Forchel, B. Ross, R. Germann, W. Heuring, and D. Grützmacher, Microelectron. Eng. **11**, 11 (1990).
[35] A. R. Long, M. Rahman, I. K. MacDonald, M. Kinsler, S. P. Beaumont, C. D. W. Wilkinson, and C. R. Stanley, Semicond. Sci. Technol. **8**, 39 (1993).
[36] B. L. Al'tshuler, A. G. Aronov, and D. E. Khmelnitsky, J. Phys. C **15**, 7367 (1982).
[37] K. K. Choi, D. C. Tsui, and K. Alavi, Phys. Rev. B **36**, 7751 (1987).
[38] S. V. Iordanskii, Y. B. Lyanda-Geller, and G. E. Pikus, JETP Lett. **60**, 206 (1994).
[39] W. Knap *et al.*, Phys. Rev. B **53**, 3912 (1996).
[40] A. V. Moroz and C. H. W. Barnes, Phys. Rev. B **61**, R2464 (2000).